Research Article | Vol. 11, No. 4 / 1 April 2020 / Biomedical Optics Express 2007
Biomedical Optics EXPRESS

# Multifunctional laser speckle imaging

E. Du, Shuhao Shen, Shau Poh Chong, and Nanguang Chen*

*Optical Bioimaging Laboratory, Department of Biomedical Engineering, National University of Singapore, 7 Engineering Drive 1, Singapore 117574, Singapore*
*biecng@nus.edu.sg

**Abstract:** We have developed a multi-functional laser speckle imaging system, which can be operated in both the surface illumination laser speckle contrast imaging (SI-LSCI) mode and the line scan laser speckle contrast imaging (LS-LSCI) mode. The system has been applied to imaging the chicken embryos to visualize both the blood flow and morphological details of the vasculature. The experimental results demonstrated that LS-LSCI is capable of detecting and quantifying blood flow in blood vessels smaller and deeper than those detectable by conventional SI-LSCI. Furthermore, the line scan mode is also capable of producing depth-resolved absorption-based morphological images of tissue, augmenting flow-based functional images.



## 1. Introduction

Laser speckle contrast imaging (LSCI) is a simple and minimally invasive optical technique for imaging blood flow in tissues since it was introduced in the 1990s [1]. In the past few decades, LSCI has been widely applied in neuroscience [2–6], dermatology [7,8] and ophthalmology [9,10]. Laser speckle is a random interference pattern produced by the coherent addition of scattered photons. If the photons are scattered by moving particles, such as moving red blood cells, the speckle pattern will change in both space and time. The spatial and temporal statistics of the speckle pattern provide information about the motion of the scattering particles. The motion can be quantified by the use of the speckle contrast. Therefore, LSCI is a useful tool for measuring blood flows.

There has been some recent progress in improving the theory, instrumentation, and applications of LSCI [11–14]. Duncan and Kirkpatrick [15] discussed the quantitative relationship between speckle contrast and flow velocity. Zakharov et. al. [16] proposed a mathematical model that took into account the presence of static particles. Parthasarathy et. al. [17] reported a Multi-Exposure Speckle Imaging instrument that can provide quantitative baseline flow measurement. They further proposed a new speckle model for better quantifying flows in the presence of static scatters. S. M. Shams Kazmi et. al. [18] argued that traditional speckle contrast imagery of vascular flows is neither a measure of volumetric flux nor particle speed, but rather the product of speed and vessel diameter. Chen et. al. [19] developed an optical method in which LSCI is combined with microendoscopy to achieve time-lapse blood flow detection in deep regions of the mice brain. W. Heeman et. al. [20] illustrated that LSCI is capable of identifying ischemic areas on the large intestine in a standard laparoscopic setup.

Nonetheless, some limitations of LSCI remain [13,14]. One major limitation is the shallow imaging depth [21]. To improve the imaging depth of LSCI, several studies have been recently reported. Bi et. al. [22] proposed a diffuse speckle contrast analysis method, which estimates the flow value based on the analysis of the speckle pattern in the spatial domain. In their imaging system, a point laser source is used and the diffuse speckle patterns at a source-detector separation distance are recorded by a CCD camera. Varma et. al. [23] proposed a speckle contrast optical tomography method that can measure the blood flow distributed in deeper regions of the tissue by scanning the point laser source over the sample and acquiring multiple speckle measurements

#388856 https://doi.org/10.1364/BOE.388856
Journal © 2020 Received 21 Jan 2020; revised 7 Mar 2020; accepted 7 Mar 2020; published 13 Mar 2020

Biomedical Optics EXPRESS

simultaneously using a CCD or CMOS camera. He et. al. [24] presented a line illumination system in an attempt to improve the sampling depth of blood flow imaging. However, their system is equivalent to a surface illumination instrument with structured light.

In this paper, we report a multi-functional Speckle Imaging system. It can be easily switched between two operation modes. One is conventional SI-LSCI with a high temporal resolution. The other mode is Line Scan Laser Speckle Contrast Imaging (LS-LSCI) with improved sensitivity to flow in deep tissue and the additional absorption-based morphological imaging capability. It is essentially a descanned imaging system with an improved ability to reject surface reflections. The instrumentation and data processing details are disclosed in the Method and Material section. Images obtained from chicken embryos are presented in Results and Discussion, in which the performance of various operation modes are compared and discussed.

## 2. Method and materials

### 2.1. Imaging setup

The schematic of the multi-functional speckle imaging system is illustrated in Fig. 1. The source is a 640 nm solid-state single-frequency laser with the coherence length > 300 m (RCL-025-640-S, CystaLaser, 25mW). A half-wave plate and a polarizing beam-splitter are used to adjust the illumination intensity on the sample. The beam is expanded using a beam expander. A cylindrical lens (ACY254-050-A, focal length 50mm) is used to condense the light in one dimension and form a line illumination. A 1-D Galvo mirror (Thorlab, GVS011) is used to provide line scanning of the beam on the sample. The back-scattered photons from the sample are collected by the lens, descanned, reflected in the detection arm by the polarizing beam-splitter to the camera. A linear polarizer is placed in front of the camera lens and its orientation is set to be perpendicular to that of the illumination beam polarization to suppress the specular reflection from the sample. The center line of the camera (Andor, Zyla 5.5 scientific CMOS) is adjusted to be conjugated to the illumination line on the sample. We use an NI PCI-6115 data acquisition card and a Labview program to synchronize the Galvo mirror and the camera.

The setup can be switched between two operation modes: one is surface illumination laser speckle contrast imaging (SI-LSCI). By removing the cylinder lens, the sample is surface illuminated and the camera is operated to record images at a speed up to 100 fps with a full image resolution of 2560 by 2160 pixels. The image acquisition speed can be further increased by reducing the filed of view. The other mode is line scan laser speckle contrast imaging (LS-LSCI), where the cylindrical lens is included in the illumination light path and the camera is operated as a line camera. In this mode, the region of interest (ROI) of the camera sensor is set to 2560 by 7 pixels. The illumination line is scanned by the Galvo mirror at 500 steps along the horizontal direction from the left to the right edge of the same imaging area as SI-LSCI. As shown in the black dashed box in Fig. 1, the optical alignment is so adjusted that the sCMOS sensor central line becomes conjugate to the illumination line. The ROI (2560 by 7 pixels) can be readily defined by the use of the Labview program. If the central lines (7 pixels in width) are chosen as an effective detection line, they are equivalent to a confocal slit detector for generating line-scan confocal images. On the other hand, sensing pixels with a preset distance from the confocal line can also be selected to function as an offset line detector, which enables more effective detection of multiple scattering photons traveling into deeper regions in a turbid medium. Furthermore, the system includes a Z- translational stage for adjusting the sample axial position. In our experiments with SI-LSCI and LS-LSCI, the camera exposure time is set to 2 ms and the field of view is set to 10.24 mm x 8.64 mm for fair comparisons. In the LS-LSCI mode, the Galvo mirror is driven by a sawtooth signal that varies as a linear function of time during each frame period. The frame acquisition time depends on the number of lines per frame. It takes 1s to acquire one LS-LSCI image consisting of 500 lines.

Biomedical Optics EXPRESS

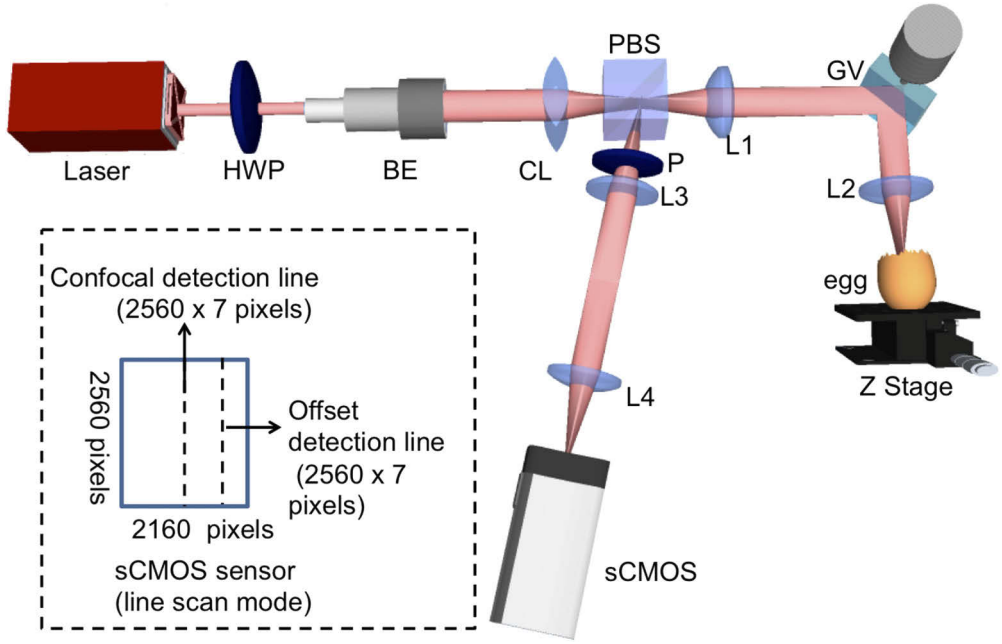


**Fig. 1.** Schematic diagram of multi-functional speckle imaging system: HWP, half-wave plate; BE, beam expander; CL, cylindrical lens; PBS, polarizing beam splitter; GV, 1-D Galvo mirror; P, polarizer. The focal length of CL was 50 mm. Focal lengths of lenses L1, L2, L3, and L4 were 50, 75, 40, and 100 mm, respectively.

### 2.2. *Algorithms for data processing*

Laser speckle contrast imaging technique is based on the measurement of intensity fluctuations of speckle patterns generated by motion in the sample recorded with a camera. The speckle contrast is simply calculated as the ratio of the standard deviation to the mean intensity,

$$K_s = \frac{\sigma_s}{\langle I \rangle}, \tag{1}$$

where $K_s$ is the spatial speckle contrast, $\sigma_s$ is the spatial standard deviation of the speckle intensity, and <I> is the mean intensity. In this paper, a square matrix of 7×7 pixels is used to compute the spatial speckle contrast images [25,26]. The speckle contrast images can be converted to velocity images using the following equations [15]:

$$K_S = \left\{ \frac{\tau_c}{2T} \left[ 2 - \frac{\tau_c}{T} (1 - e^{-2T/\tau_c}) \right] \right\}^{1/2} \tag{2}$$

$$\upsilon = \frac{\lambda/2\pi}{\tau_c} \tag{3}$$

Here T is the exposure time of the camera, $\tau_c$ is the correlation time, $\lambda$ is the wavelength of the laser, and $\upsilon$ is the flow velocity. According to Eqs. (2) and (3), the speckle contrast $K_s$ and the flow velocity $\upsilon$ are related inversely. Hence, in speckle contrast images blood vessels carrying flow appear as darker regions against a lighter background. For faster speeds, $K_s$ becomes smaller and vice versa. Note that the flow velocity only provides the numerical value of the flow velocity without direction information.

Biomedical Optics EXPRESS

### 2.3. Sample preparation

Fertilized chicken eggs were obtained from a local poultry farm (Lian Wah Hang Farm PTE LTD, Singapore). The eggs were incubated at 38.5°C and 75% humidity. On embryonic day 3 (Hamburger-Hamilton stage 18), a blunt forceps was used to puncture a hole on the top where the air pocket was located. Then the shell membrane was removed with sharp forceps until the entire embryo can be seen. After imaging experiments, the eggs can be put back into the incubator. Chicken embryos on the 3rd day through the 5th day of incubation were imaged. All the experiments conducted have been reviewed and approved by the Institutional Animal Care and Use Committee (IACUC) of the National University of Singapore.

## 3. Results and discussion

### 3.1. LS-LSCI with confocal detection

To demonstrate the advantages of LS-LSCI, we have conducted experiments to compare the imaging performances, in terms of contrast and spatial resolution, between conventional SI-LSCI and LS-LSCI. Figure 2(a) shows the blood flow velocity image of a day 3 chicken embryo obtained with SI-LSCI. Figure 2(b) shows the blood flow velocity image of the same chicken embryo obtained with LS-LSCI, for which confocal line detection was used. The magnified views of the yellow dashed box in images 2(a) and 2(b) are displayed in Fig. 2(c) and 2(d), respectively. Plotted in Fig. 2(e) are example intensity profiles taken along the same line in Figs. 2(c) and 2(d), indicated in blue and red, respectively. Comparing the images and line profiles, it is apparent that blood flow in some small vessels cannot be well differentiated from the background in the SI-LSCI image, but can be visualized and quantified by LS-LSCI with much-improved contrast and effective spatial resolution.

We have further investigated the performance of the two operation modes in visualizing blood flow in the microvasculature. In Figs. 3(a) and 3(b) we compare the speckle contrast images of a partial chicken embryo (day 5) obtained by SI-LSCI and LS-LSCI, respectively. The speckle contrast instead of blood velocity is used here as it provides a clearer visualization of the microvasculature morphology. Figures 3(a) and 3(b) are displayed using grey scales of 0 to 0.3 and 0 to 0.4, respectively. One can see that some small vessels (in the yellow circled regions) are clearly visible in the LS-LSCI image but can hardly be seen in the SI-LSCI image due to poor contrast. The LS-LSCI image reveals much detailed and high-resolution vascular features than the SI-LSCI image. The finest vessels discernible in LS-LSCI images are roughly 40 microns in diameter. More importantly, blood flow in these microvessels can be better localized, quantified, and differentiated from the surrounding tissue in the LS-LSCI image.

It is well known that conventional SI-LSCI is a non-scanning imaging technique, which inclusively integrates information from various depths to generate a 2D map of the field of view [12]. We believe that the improved contrast and spatial resolution in LS-LSCI are achieved by the use of line illumination and confocal line detection, which are combined to enhance sensitivity to local flow. Similar to its fluorescence microscopy and optical coherence tomography counterparts, the line scan confocal laser speckle imaging method enjoys the intrinsical optical sectioning capability [29–31].

### 3.2. LS-LSCI with offset line detection

While confocal detection affords the desired transverse and axial resolutions, it is found that such a configuration is highly sensitive to surface specular reflection. In addition, its imaging depth is usually limited to a few hundred microns. In order to probe blood flow in regions deeper than 1 mm, our LS-LSCI system allows line detection at a distance from the confocal line. The improved penetration depth can be explained by the photon migration theory [27]. The trajectories of photons propagating in a turbid medium are usually “banana” shaped and multiple scattering

Biomedical Optics EXPRESS

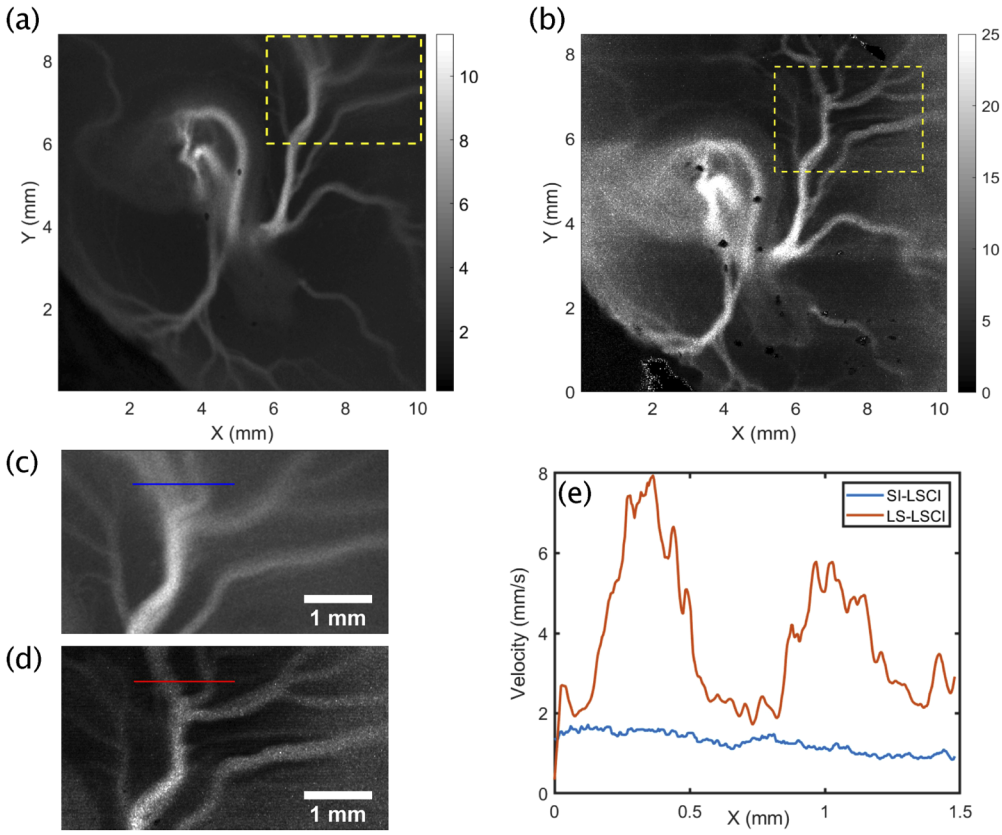


**Fig. 2.** Blood flow velocity maps of a chicken embryo (day 3) obtained with (a) SI-LSCI (averaged over 30 frames) and (b) LS-LSCI using the confocal line detector (averaged over 30 frames); (c) and (d) are magnified views of the yellow dashed boxed regions in (a) and (b), respectively; (e) line profiles along the blue line in (c) and red line in (d).

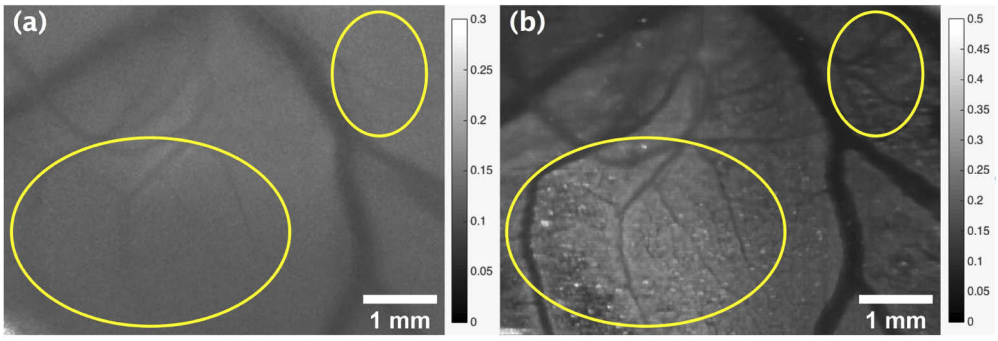


**Fig. 3.** The speckle contrast images of a partial chicken embryo (day 5) using the (a) SI-LSCI (b) LS-LSCI with the confocal line detector. The circled vessels (the yellow regions) are more visible in (b) compared to (a).

Biomedical Optics EXPRESS

photons traveling for a longer distance generally probe a larger volume [27]. Therefore, as the source-detector separation increases, the penetration depth can be enhanced [28]. Of course, the spatial resolution will deteriorate at the same time. In our LS-LSCI experiments with offset line detection, the source-detector separation is chosen empirically to compromise between imaging depth and spatial resolution.

Provided in Fig. 4 are speckle contrast images of the same chicken embryo in Fig. 3 obtained by LS-LSCI with a source-detector separation of 0.2 mm. They were acquired when the focal plane was shifted from the embryo surface to 3 mm in depth, at an increment of 1 mm. In the surface image (Fig. 4(a)), small superficial vessels in the yellow circle are still visible, but with a reduced spatial resolution of around 0.2 mm. As the imaging depth increases, the vessels in the same region fade gradually (Figs. 4(b) to 4(d)). On the other hand, blood flow in the red rectangle can be best seen at a depth of 2 mm (see Fig. 4(c)) but is absent in Fig. 4(a).

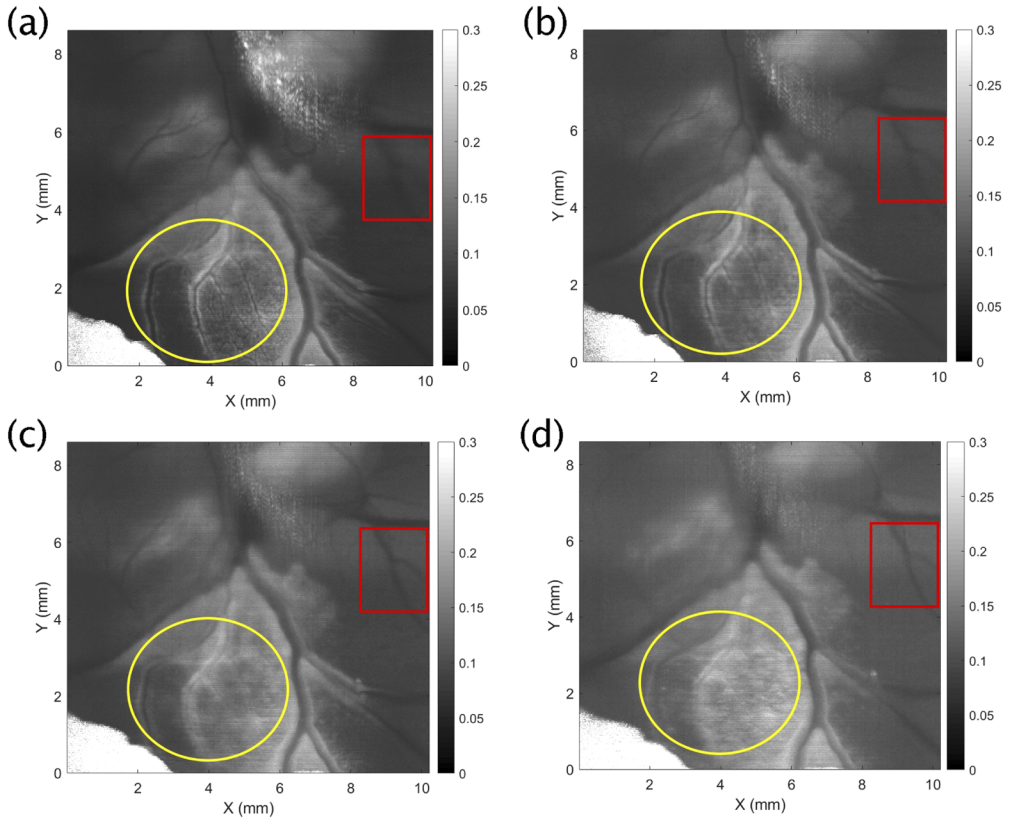


**Fig. 4.** Laser speckle contrast images of a partial chicken embryo (day 5) using LS-LSCI with a source–detector separation of 0.2mm. They are obtained when locating the focal plane (a) on the surface, (b) 1mm beneath the surface, (c) 2mm beneath the surface, and (d) 3 mm beneath the surface.

### *3.3. High temporal resolution of SI-LSCI*

The emphasis of this paper is to demonstrate improved spatial resolution, penetration depth, and flow quantification of LS-LSCI. However, we still keep SI-LSCI as an option as it can provide a better temporal resolution. A high temporal resolution could be desirable in certain situations.

While the laser speckle contrast imaging technology cannot directly provide the blood flow direction, here we demonstrate that the high temporal resolution of SI-LSCI enables proper

Biomedical Optics EXPRESS

differentiation between arterial and venous flows in the chicken embryo. Using SI-LSCI, a blood flow velocity movie (**Visualization 1**) consisting of 100 continuous frames was obtained at an imaging speed of 100 fps. Figures 5(a) and 5(b) are representative frames from the movie, corresponding to blood flow at the time points 0.61s and 0.98s, respectively. Figures 5(a) and (b) are merged to form Fig. 5(c) in which the vessels are pseudo-colored in red and blue, respectively. Enclosed in the dashed yellow circle is the heart of the chicken embryo (Day 3). Figure 5(d) shows the time courses of the flow velocity at the vessels marked by the white squares in Fig. 5(c). It is obvious that the blood flow in red vessels pulsing with the heart beating is the arterial blood flow and the relative stationary blood flow in the blue vessels is venous. Therefore, based on temporal flow dynamics, the high temporal resolution of SI-LSIC can be used to differentiate arterial and venous flows.

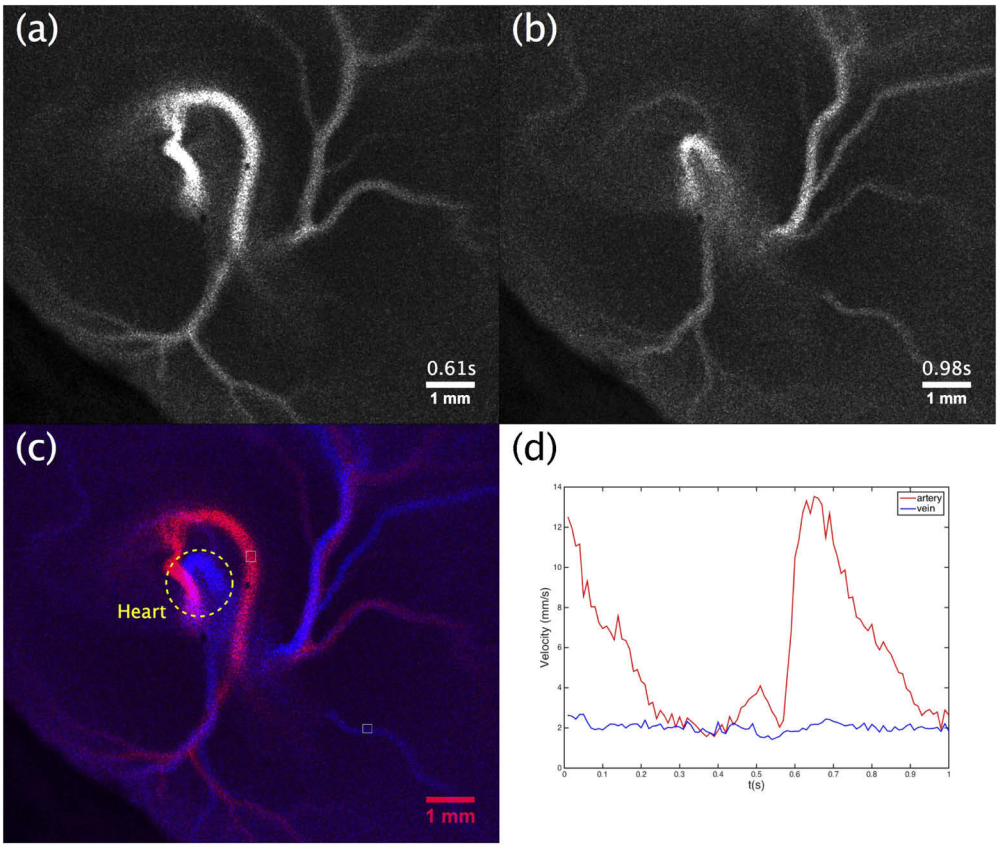


**Fig. 5.** The blood flow velocity images of the chicken embryo (day 3) using SI-LSCI. (a) the arterial blood flow at time point 0.61s (b) the venous blood flow at time point 0.98. (c) Merged image from arterial blood flow (red) and venous blood flow (blue), yellow dashed circled region is the heart.(d) Time courses of the blood flow at the positions indicated by the two white squares marked regions in (c).

### *3.4. Absorption-based morphological imaging*

Other than functional imaging in terms of blood flow, our multi-functional laser speckle contrast imaging system provides an extra function of absorption-based morphological imaging. Here we demonstrate that LS-LSCI, especially LS-LSCI with offset line detection, can be employed to visualize tissue morphology at different depths.

Biomedical Optics EXPRESS

In Fig. 6 we compare time averaged (over 30 consecutive frames) images obtained with various illumination and detection configurations. Speckles in single frames have been essentially averaged out, resulting in intensity images where absorbing features appear dark. Figure 6(a) shows the averaged SI-LSCI images of a day 4 chicken embryo. The embryo is covered by a strongly scattering white membrane. As a result, most detailed features underneath the membrane are masked and only the eye is visible. Figures 6(b)-(d) are averaged LS-LSCI images with confocal line detection and offset line detection at 0.2 mm and 2 mm, respectively. The confocal image (Fig. 6(b)) reveals a lot of high-resolution superficial structures including small blood vessels. However, it is difficult for the confocal imaging mode to overcome strong specular reflection in a big area (enclosed in the dashed yellow line). Specular reflection is noticeable and annoying in other smaller regions as well. With adequately large source-detection separations in the line scan mode, deep morphology is no longer masked by the surface membrane and specular reflection. By increasing the source-detector separation, it is possible to visualize structures in deeper regions.

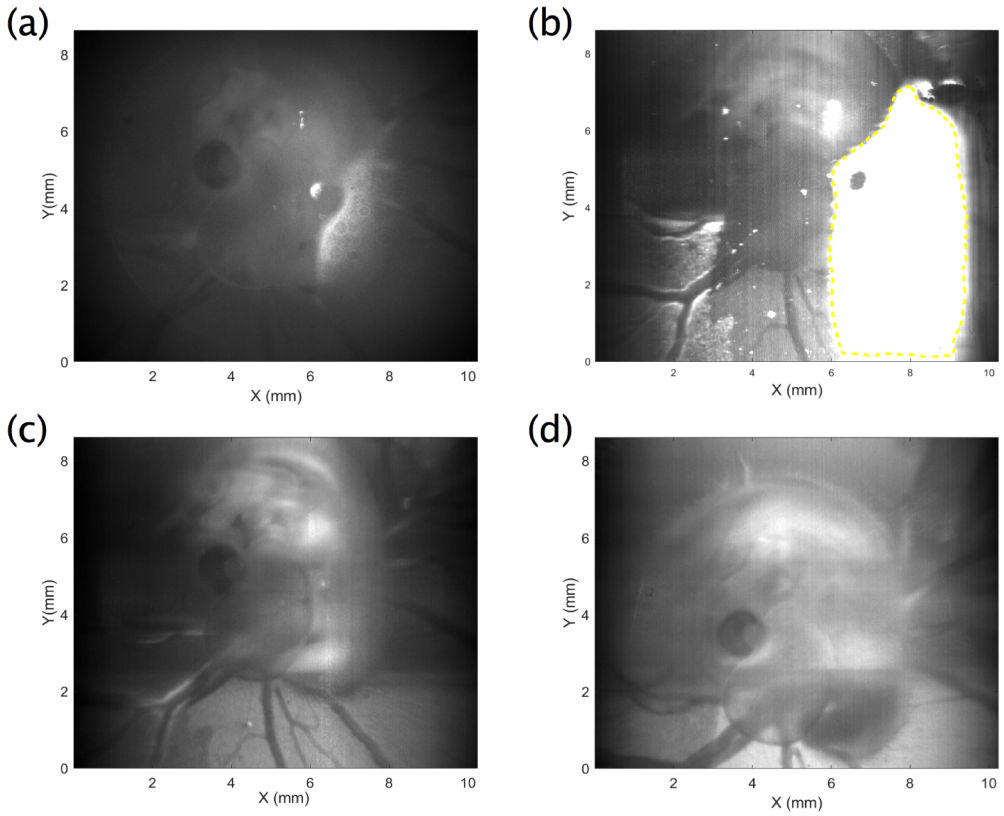


**Fig. 6.** The morphological images of a chicken embryo (day 4) obtained using (a) SI-LSCI, (b) LS-LSCI with confocal line detection, (c) LS-LSCI with offset line detection at 0.2 mm, and (d) LS-LSCI with offset line detection at 2 mm.

### *3.5. Future directions*

In this work, the performance of the multi-functional laser speckle imaging system is validated with chicken embryos in their early development stages. In the future, we will explore other potential applications of this technique. For example, the mouse brain has been widely used

Biomedical Optics EXPRESS

as a tumor model and traditional SI-LSCI has been employed to visualize the vasculature and blood flow. We expect that LS-LSCI could afford better flow quantification, spatial resolution, and penetration depth. However, the brain tissue is more scattering than the early stage chicken embryos. We probably need to switch to a near infrared laser (of a longer wavelength) to reduce the scattering effects and achieve the expected performance enhancements. Application of LS-LSCI to human skin imaging is also of great interest. To acquire in vivo images from human subjects, there is an additional challenge other than the strong scattering of the skin. The frame rate of our current LS-LSCI is around 1 Hz, which makes is sensitive to motion artefacts. A significant reduction in the line exposure time and/or the number of lines per frame would be necessary.

## 4. Conclusion

In summary, we have built a multi-functional laser speckle imaging system, which can be conveniently switched between two flow imaging modes. One is conventional Surface Illumination Laser Speckle Contrast Imaging (SI-LSCI), which is capable of monitoring dynamic changes in blood flow attributed to its high temporal resolution. The other mode is Line Scan Laser Speckle Contrast Imaging (LS-LSCI), which can provide significantly improved image contrast and depth resolution. Additionally, the line scan imaging mode is capable of producing morphological images of tissue at different depths by adjusting the source-detector separation.

## Funding

Ministry of Education - Singapore (R-397-000-327-114).

## Acknowledgments

We would like to thank Prof. Yap Choon Hwai and Mr. Zhen Yu Gordon Ko for their assistance in sample preparation.

## Disclosures

The authors declare that there are no conflicts of interest related to this article.

## References

1. A. Fercher and J. Briers, "Flow visualization by means of single-exposure speckle photography," Opt. Commun. **37**(5), 326–330 (1981).
2. H. Bolay, U. Reuter, A. K. Dunn, Z. Huang, D. A. Boas, and M. A. Moskowitz, "Intrinsic brain activity triggers trigeminal meningeal afferents in a migraine model," Nat. Med. **8**(2), 136–142 (2002).
3. P. Li, S. Ni, L. Zhang, S. Zeng, and Q. Luo, "Imaging cerebral blood flow through the intact rat skull with temporal laser speckle imaging," Opt. Lett. **31**(12), 1824–1826 (2006).
4. P. Zakharov, A. C. Völker, M. T. Wyss, F. Haiss, N. Calcinaghi, C. Zunzunegui, A. Buck, F. Scheffold, and B. Weber, "Dynamic laser speckle imaging of cerebral blood flow," Opt. Express **17**(16), 13904–13917 (2009).
5. A. Parthasarathy, S. M. Shams Kazmi, and A. Dunn, "Quantitative imaging of ischemic stroke through thinned skull in mice with Multi Exposure Speckle Imaging," Biomed. Opt. Express **1**(1), 246–259 (2010).
6. A. K. Dunn, "Laser Speckle Contrast Imaging of Cerebral Blood Flow," Ann. Biomed. Eng. **40**(2), 367–377 (2012).
7. J. D. Briers and S. Webster, "Laser speckle contrast analysis_LASCA : a nonscanning, full-field technique for monitoring capillary blood flow," J. Biomed. Opt. **1**(2), 174–179 (1996).
8. B. Choi, N. M. Kang, and J. S. Nelson, "Laser speckle imaging for monitoring blood flow dynamics in the in vivo rodent dorsal skin fold model," Microvasc. Res. **68**(2), 143–146 (2004).
9. J. D. Briers and A. F. Fercher, "Retinal blood-flow visualization by means of laser speckle photography," Invest. Ophthalmol. Visual Sci. **22**(2), 158–161 (1982).
10. Haiying Cheng, Yumei Yan, and Timothy Q. Duong, "Temporal statistical analysis of laser speckle images and its application to retinal blood-flow imaging," Opt. Express **16**(14), 10214–10219 (2008).
11. David A. Boas and Andrew K. Dunn, "Laser speckle contrast imaging in biomedical optics," J. Biomed. Opt. **15**(1), 011109 (2010).

Biomedical Optics EXPRESS


12. Janaka Senarathna, Abhishek Rege, Nan Li, and Nitish V. Thakor, "Laser Speckle Contrast Imaging: Theory, Instrumentation and Applications," IEEE Rev. Biomed. Eng. **6**, 99–110 (2013).
13. D. Briers, D. Duncan, S. Kirkpatrick, M. Larsson, T. Stromberg, and O. Thompson, "Laser speckle contrast imaging: Theoretical and practical limitations," J. Biomed. Opt. **18**(6), 066018 (2013).
14. Pedro G. Vaz, Anne Humeau-Heurtier, Edite Figueiras, Carlos Correia, and Joao Cardoso, "Laser Speckle Imaging to Monitor Microvascular Blood Flow: A Review," IEEE Rev. Biomed. Eng. **9**, 106–120 (2016).
15. D. D. Duncan and S. J. Kirkpatrick, "Can laser speckle flowmetry be made a quantitative tool?" J. Opt. Soc. Am. A **25**(8), 2088–2094 (2008).
16. P. Zakharov, A. Völker, A. Buck, B. Weber, and F. Scheffold, "Quantitative modeling of laser speckle imaging," Opt. Lett. **31**(23), 3465–3467 (2006).
17. A. Parthasarathy, W. Tom, A. Gopal, X. Zhang, and A. Dunn, "Robust flow measurement with multi-exposure speckle imaging," Opt. Express **16**(3), 1975–1989 (2008).
18. S. M. Shams Kazmi, E. Faraji, M. A. Davis, Yu-Yen Huang, Xiaojing J. Zhang, and Andrew K. Dunn, "Flux or speed? Examining speckle contrast imaging of vascular flows," Biomed. Opt. Express **6**(7), 2588–2608 (2015).
19. M. Chen, D. Wen, S. Huang, S. Gui, Z. Zhang, J. Lu, and P. Li, "Laser speckle contrast imaging of blood flow in the deep brain using microendoscopy," Opt. Lett. **43**(22), 5627–5630 (2018).
20. W. Heeman, K. Dijkstra, C. Hoff, S. Koopal, J. Pierie, H. Bouma, and E. C. Boerma, "Application of laser speckle contrast imaging in laparoscopic surgery," Biomed. Opt. Express **10**(4), 2010–2019 (2019).
21. J. ODoherty, P. McNamara, N. Clancy, J. Enfield, and M. Leahy, "Comparison of instruments for investigation of microcirculatory blood flow and red blood cell concentration," J. Biomed. Opt. **14**(3), 034025 (2009).
22. R. Bi, J. Dong, and K. Lee, "Deep tissue flowmetry based on diffuse speckle contrast analysis," Opt. Lett. **38**(9), 1401–1403 (2013).
23. H. M. Varma, C. P. Valdes, A. K. Kristoffersen, J. P. Culver, and T. Durduran, "Speckle contrast optical tomography: A new method for deep tissue three-dimensional tomography of blood flow," Biomed. Opt. Express **5**(4), 1275–1289 (2014).
24. H. He, Y. Tang, F. Zhou, J. Wang, Q. Luo, and P. Li, "Lateral laser speckle contrast analysis combined with line beam scanning illumination to improve the sampling depth of blood flow imaging," Opt. Lett. **37**(18), 3774–3776 (2012).
25. J. D. Briers, G. Richards, and X. W. He, "Capillary blood flow monitoring using laser speckle contrast analysis (LASCA)," J. Biomed. Opt. **4**(1), 164–175 (1999).
26. A. K. Dunn, H. Bolay, M. A. Moskowitz, and D. A. Boas, "Dynamic imaging of cerebral blood flow using laser speckle," J. Cereb. Blood Flow Metab. **21**(3), 195–201 (2001).
27. S. Feng and F. Zeng, "Monte Carlo simulations of photon migration path distributions in multiple scattering media," Proc. SPIE **1888**, 78–89 (1993).
28. Andrew Dunn and David Boas, "Transport-based image reconstruction in turbid media with small source– detector separations," Opt. Lett. **25**(24), 1777–1779 (2000).
29. S. Pant, Y. Duan, F. Xiong, and N. Chen, "Augmented line-scan focal modulation microscopy for multi-dimensional imaging of zebrafish heart in vivo," Biomed. Opt. Express **8**(12), 5698–5707 (2017).
30. S. Pant, C. Li, Z. Gong, and N. Chen, "Line-scan focal modulation microscopy," J. Biomed. Opt. **22**(5), 050502 (2017).
31. Z. Al-Qazwini, Z. Y. G. Ko, K. Mehta, and N. Chen, "Ultrahigh-speed line-scan SD-OCT for four-dimensional in vivo imaging of small animal models," Biomed. Opt. Express **9**(3), 1216–1228 (2018).